IEEE Access
Multidisciplinary | Rapid Review | Open Access Journal

Received June 23, 2020, accepted July 2, 2020, date of publication July 6, 2020, date of current version July 23, 2020.

Digital Object Identifier 10.1109/ACCESS.2020.3007444

The Charging Control and Efficiency Optimization Strategy for WPT System Based on Secondary Side Controllable Rectifier

MING ZHANG, (Graduate Student Member, IEEE), LINLIN TAN, JIACHENG LI, (Student Member, IEEE), AND XUELIANG HUANG, (Member, IEEE)

School of Electrical Engineering, Southeast University, Nanjing 210096, China
Key Laboratory of Smart Grid Technology and Equipment in Jiangsu Province, Nanjing 210096, China

Corresponding author: Linlin Tan (tanlinlin@seu.edu.cn)

This work was supported by the National Key Research and Development Project under Grant 2018YFB0106300.

ABSTRACT The equivalent resistance of the battery will change during charging in practical applications, so it is difficult to design a wireless power transfer (WPT) system with accurate constant current (CC) and constant voltage (CV) output characteristics. In addition, the WPT system efficiency is also affected by the change of equivalent resistance. Therefore, this paper studies the charging control and efficiency optimization strategy for the WPT system with dynamic loads. The WPT system with a structure of double-sided LCC compensation topology and containing controllable rectifier circuit at the secondary side is established, and the working process of full-bridge controllable rectifier circuit is analyzed. Then the output characteristics of the WPT system are analyzed. The expressions of the optimal transmission efficiency and the optimal equivalent impedance of the full-bridge rectifier are derived. The relationships between the equivalent impedance of the capacitor-filtered full-bridge controllable rectifier circuit and the phase shift angle, the charging current and the phase shift angle are also obtained. In this paper, the CC and CV charging strategies based on phase shift control of controllable rectifier circuit and efficiency optimization strategy based on dynamic equivalent impedance matching are proposed, which can improve the WPT system transmission efficiency while realizing CC and CV charging. Finally, the effectiveness of the proposed control strategy is verified by simulation and experiment. The WPT system realizes CC charging mode and CV charging mode in turn when the load resistance changes from 5 Ω to 30 Ω, and the overall efficiency is up to 90.71% at the transmission distance of 15cm.

INDEX TERMS Wireless power transfer, constant current/voltage charging, efficiency optimization, phase shift control, dynamic impedance matching.

I. INTRODUCTION

The WPT technology can effectively help the electrical equipment to get rid of the shackles of cables and improve the flexibility and safety of electricity [1], [2]. At present, it has been applied in electric vehicles, portable electronic devices, medical implant, drones, inspection robots, etc. References [3]–[6]. In recent years, electric vehicles have developed rapidly, and the wireless charging technology for electric vehicles based on the principle of WPT has emerged at the historic moment in order to solve several problems existing in wired electric energy supplement [7].

In practical applications, the lithium batteries are widely used in electric vehicles. In order to extend the life cycle of batteries, two modes of CC and CV are generally adopted during the charging process. However, the equivalent resistance of the battery gradually increases during the charging process which will have a certain impact on the output characteristics of the WPT system. For example, the actual charging current or charging voltage may deviate from the battery demand value and the overall efficiency may be lower, which is a big challenge for the design and control of the WPT system [8]–[10]. In order to solve the above problems,

The associate editor coordinating the review of this manuscript and approving it for publication was Jun Shen.

the charging control method of the WPT system has been studied by many scholars. The main methods include phase-shifting modulation (PSM) control or frequency conversion control (FCC) of the primary side high-frequency inverter (HFI), resonant compensation circuit design and control, and addition of a DC-DC converter, etc. [11]–[17].

The authors of [18] developed a control strategy based on dual-phase-shift control with an active rectifier to maintain a constant output voltage or current. The PSM technology based on HFI can guarantee constant current output or constant voltage output. However, it must be built on the premise that the primary side and the secondary side have reliable communication. The feasibility of this method is not high when the load resistance value changes significantly. This method may not be feasible when the load resistance changes significantly. The authors of [19] analyzed the frequency characteristics of the double-sided LCC compensation tank to achieve both of load-independent current and voltage characteristics with the ZPA condition at two different resonant frequencies. The FCC technology can realize the CC/CV charging mode independent of the load theoretically. The adjustable range of frequency is limited in the WPT system, resulting in the method being not flexible and versatile. In Ref. [20], a mixed high-order compensation networks is proposed to achieve multiple independent outputs with constant currents. A LC/S compensation topology is proposed in Ref. [21] to provide excellent CC out characteristic. The authors of [22] analyzed and summarized the individual passive resonant networks used to achieve CC or CV output characteristics against the time-varying load. In Ref. [23], the three-coil structure WPT system is proposed to achieve stable CC and CV charging output characteristics for battery charging applications. An LCL-network-based SS compensated in Ref. [24] is proposed to achieve adjustable output current and wide ZVS range. In Ref. [25], integrated control method of load estimation and power tracking are proposed to achieve CC/CV charging of LCC compensation WPT system. In the paper of [26], a general modeling methods for the high-order resonant circuit is proposed to investigate the load-independent voltage and current transfer characteristics. These studies can realize the control of CC or CV output on the design of different resonant compensation structures. However, this method may be less compatible with different types of loads. In addition, the extra loss caused by the large number of components will reduce the overall efficiency of the WPT system to some extent. The authors of [27] propose a series-series compensated WPT system based on parity-time symmetry with front-end DC-DC converter and a primary-side-only control strategy in order to attain stable output power with high transfer efficiency under various coupling condition and load. For the method of adding DC-DC converter, the charging control of CC or CV can be realized, and the flexibility is higher. However, this method will increase the weight and volume of the system, and the overall efficiency will be reduced due to the loss of the DC-DC converter itself.

In order to overcome the disadvantages of the above control methods such as inflexibility, poor compatibility, increased weight and volume and influence on efficiency, this paper proposes the control method of CV/CC charging and the optimization strategy of efficiency for the change of equivalent load resistance. The WPT system with a structure of double-sided LCC compensation topology and containing controllable rectifier circuit at the secondary side are studied. By analyzing the output characteristics of the WPT system and deriving the relationship between the charging current and phase shift angle, a CC/CV charging model control strategy based on the controllable rectifier circuit through the phase-shifting control is proposed. The open loop control is adopted for the CC charging model on the premise of satisfying the precision in order to respond the load demand quickly. The CV charging model adopts closed-loop control, and the whole charging process does not require communication between the secondary side and the primary side. Then, an efficiency optimization strategy based on dynamic equivalent impedance matching is proposed by deducing the relationship between equivalent impedance of rectifier circuit and transmission efficiency. This paper consists of six sections. The arrangement of the remaining sections is as follows: section II describes the structure of the WPT system, analyzes the working process and obtains the output characteristics through theoretical analysis. Section III proposes the CC/CV control method and efficiency optimization strategy. Section IV verifies the effectiveness and reliability of the proposed charging control strategy through simulation and experiment. In the last section, the conclusions drawn from the research are summarized.

II. THE WPT SYSTEM STRUCTURE AND THEORETICAL ANALYSIS

A. THE WPT SYSTEM STRUCTURE AND WORKING PROCESS

In this paper, a structure of double-sided LCC compensation topology is taken as an example to analyze the WPT system. The WPT system with a structure of double-sided LCC compensation topology and containing full-bridge controllable rectifier circuit at the secondary side is shown in Figure 1. The input voltage $\boldsymbol{U}_{\mathrm{i}}$ of the system is a high frequency sinusoidal wave, and the operating frequency of the system is f_{o} (The angular frequency $\omega = 2\pi f_{\mathrm{o}}$, the working period $T = 1/f_{\mathrm{o}}$).

The transmitter coil and receiver coil are L_{t} and L_{r} respectively, and the internal resistances are R_{t} and R_{r} respectively. M represents mutual inductance between transmitter coil and receiver coil. The primary side LCC resonance compensation topology consists of L_1-C_1-C_{t}, and the secondary side LCC resonance compensation topology consists of L_2-C_2-C_{r}. The secondary side controllable rectifier circuit is composed of four Power MOSFETs (V_1-V_4). C_{f} is the filter capacitance, and the load equivalent resistance R_{L} is composed of a battery and a resistor.

The AC side voltage and current of the rectifier circuit are $\boldsymbol{U}_{\mathrm{a}}$ and $\boldsymbol{I}_{\mathrm{a}}$ (effective values are U_{am} and I_{am}) respectively,

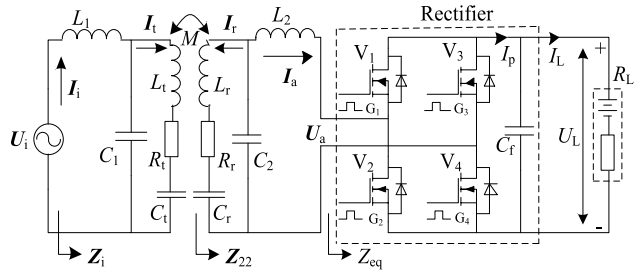

FIGURE 1. The WPT system with a structure of double-sided LCC compensation topology and containing controllable rectifier circuit at the secondary side.

the current before capacitor filtering is $\boldsymbol{I}_p$, and the DC side voltage and current are U_L and I_L respectively. Suppose the equivalent impedance of the capacitive filter type full-bridge controllable rectifier circuit is Z_{eq}. In a system working period, the full-bridge controllable rectifier circuit will have four working states:

State 1: The current flowing through $\boldsymbol{U}_a$-V_1-V_3 loop, and the working time is $0 \sim t_1$, as shown in Figure 2(a).

State 2: The current flowing through $\boldsymbol{U}_a$-V_1-R_L-V_4 loop, and the working time is $t_1 \sim T/2$, as shown in Figure 2(b).

State 3: The current flowing through $\boldsymbol{U}_a$-V_4-V_2 loop, and the working time is $T/2 \sim t_2$, as shown in Figure 2(c).

State 4: The current flowing through $\boldsymbol{U}_a$-V_3-R_L-V_2 loop, and the working time is $t_2 \sim T$, as shown in Figure 2 (d).

B. ANALYSIS OF OUTPUT CHARACTERISTICS FOR THE WPT SYSTEM

For the WPT system with a structure of double-sided LCC compensation topology, the equivalent impedance $\boldsymbol{Z}_{22}$ of the secondary side circuit can be deduced when the system is in resonance state [28], [29].

$$\boldsymbol{Z}_{22} = \frac{\omega^2 L_2^2}{Z_{eq}} + R_r \tag{1}$$

The reflected impedance $\boldsymbol{Z}_{ref}$ from the secondary side to the primary side is:

$$\boldsymbol{Z}_{ref} = \frac{(\omega M)^2}{\boldsymbol{Z}_{22}} = \frac{M^2 Z_{eq}}{L_2^2 + R_r Z_{eq}/\omega^2} \tag{2}$$

Then, the input impedance $\boldsymbol{Z}_i$ and input current $\boldsymbol{I}_i$ of the WPT system can be obtained respectively, as shown in (3) and (4).

$$\boldsymbol{Z}_i = \frac{\omega^2 \cdot L_1^2}{R_t + \boldsymbol{Z}_{ref}} \tag{3}$$

$$\boldsymbol{I}_i = \frac{C_1 \boldsymbol{U}_i (R_t + \boldsymbol{Z}_{ref})}{L_1} \tag{4}$$

Equation (5) and (6) are the current flowing through the transmitter coil and receiver, respectively.

$$\boldsymbol{I}_t = \frac{\boldsymbol{U}_i}{j\omega L_1} \tag{5}$$

$$\boldsymbol{I}_r = -\frac{M\boldsymbol{U}_i}{L_1(\omega^2 L_2^2/Z_{eq} + R_r)} \tag{6}$$

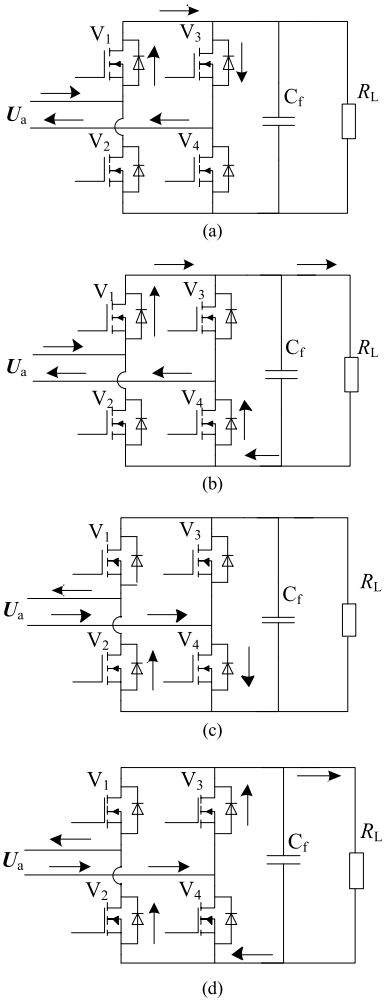

FIGURE 2. The working states of the full-bridge controllable rectifier circuit in one cycle. (a) $0 \sim t_1$: U_a-V_1-V_3 loop. (b) $t_1 \sim T/2$: U_a-V_1-R_L-V_4 loop. (c) $T/2 \sim t_2$: U_a-V_4-V_2 loop. (d) $t_2 \sim T$: U_a-V_3-R_L-V_2 loop.

Furthermore, the current $\boldsymbol{I}_a$ on the AC side of the rectifier circuit is derived as:

$$\boldsymbol{I}_a = \frac{M\boldsymbol{U}_i}{j\omega L_1(L_2 + C_2 R_r Z_{eq})} \tag{7}$$

Equation (7) can be simplified as (8) if the internal resistance R_r of the receiver coil is ignored.

$$\boldsymbol{I}_a = \frac{M\boldsymbol{U}_i}{j\omega L_1 L_2} \tag{8}$$

It can be seen from (8) that the phase difference between $\boldsymbol{I}_a$ and $\boldsymbol{U}_i$ is 90 degrees and the WPT system with the double-side LCC resonance compensation topology has the constant current output characteristic in the resonant state. So the phase of the primary side electrical parameter can be obtained indirectly by detecting the secondary side electrical parameter. The expression for mutual inductance M from (8) is:

$$M = \frac{\omega L_1 L_2 I_{am}}{U_{im}} \tag{9}$$

Suppose t_1 in Figure 2 satisfy (10), then the conduction angle is 2α. According to the characteristics of the full-bridge

rectifier circuit of the capacitor filter (voltage source drive) type, the relationship between the AC side current $\boldsymbol{I}_a$ and the DC side current I_L is show in (11):

$$t_1 = \frac{T}{2} - \frac{\alpha T}{\pi} \tag{10}$$

$$I_L = \frac{1}{\pi}\int_{\pi-2\alpha}^{\pi} \sqrt{2} I_{am} \sin(\omega t) d(\omega t) = \frac{\sqrt{2}(1-\cos 2\alpha)}{\pi} I_{am} \tag{11}$$

The charging voltage U_L and charging power P_L can be obtained from (11), as shown in (12) and (13) respectively.

$$U_L = \frac{\sqrt{2}(1-\cos 2\alpha) I_{am}}{\pi} R_L \tag{12}$$

$$P_L = \frac{2M^2 U_{im}^2 (1-\cos 2\alpha)^2}{\pi^2 \omega^2 L_1^2 L_2^2} R_L \tag{13}$$

It can be known from (13) that the charging power is positively related to the equivalent resistance of the load. Without neglecting the internal resistance of the transmitter coil and the receiver coil, the transmission efficiency η_t of the WPT system can be deduced as:

$$\eta_t = \frac{M^2}{\frac{R_t L_2^2}{Z_{eq}} + (R_t C_2^2 R_r^2 + \frac{M^2 C_2 R_r}{L_2}) Z_{eq} + 2L_2 C_2 R_t R_r + M^2} \tag{14}$$

When the equivalent impedance Z_{eq} satisfies (15), the maximum transmission efficiency of the system is η_m, as shown in (16).

$$Z_{eq\_m} = \sqrt{\frac{R_t L_2^4 \omega^2}{R_r (R_t R_r/\omega^2 + M^2)}} \tag{15}$$

$$\eta_m = \frac{1}{2\left(\sqrt{\frac{R_t^2 R_r^2 L_2^2 C_2^2}{M^4} + \frac{R_t R_r L_2 C_2}{M^2}} + \frac{R_t R_r L_2 C_2}{M^2}\right) + 1} \tag{16}$$

When the conduction angle of the rectifier circuit is unchanged, the curves of charging power P_L and transmission efficiency η_t as a function of the equivalent impedance Z_{eq} can be obtained as shown in Figure 3.

Assuming that the power factor of capacitive-filtered full bridge rectifier circuit is λ, and the expression of the power factor after Fourier analysis is as follows [30].

$$\lambda = \frac{\sqrt{2}\left(\alpha - \frac{1}{2}\sin 2\alpha\right)}{\sqrt{\pi\left(\alpha - \frac{3}{2}\sin 2\alpha + 2\alpha\cos^2\alpha\right)}} \tag{17}$$

Without considering the loss of rectifier circuit, the active power on the AC side is equal to the power on the DC side, which is the relationship shown in (18).

$$U_{am} \cdot I_{am} \cdot \lambda = U_L \cdot I_L \tag{18}$$

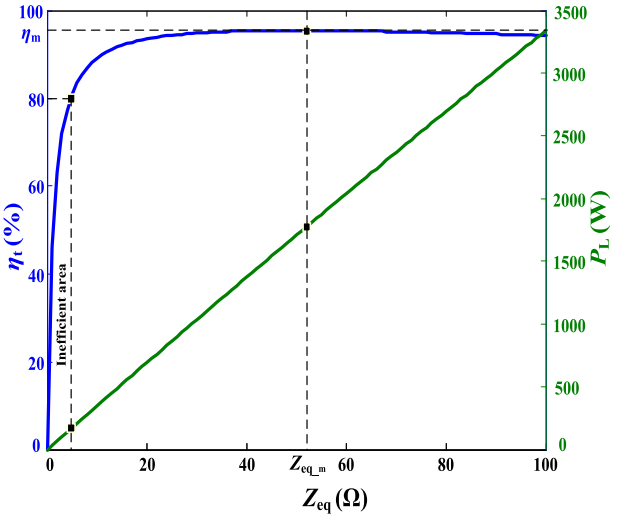

FIGURE 3. The curves of charging power P_L and transmission efficiency η_t as a function of the equivalent impedance Z_{eq}.

Then, the equivalent impedance Z_{eq} of capacitive-filtered type full bridge controllable rectifier can be obtained as:

$$Z_{eq} = \frac{2(1-\cos 2\alpha)^2}{\pi^2 \lambda} R_L \tag{19}$$

$$Z_{eq} = (0 \sim 8/\pi^2) R_L \tag{20}$$

Therefore, the range of equivalent impedance Z_{eq} is as shown in (20), which also indicates that t Z_{eq} is less than the equivalent resistance of the load.

III. THE CHARGING CONTROL AND EFFICIENCY OPTIMIZATION STRATEGY FOR DYNAMIC LOAD

A. THE CC/CV CONTROL STRATEGY BASED ON CONTROLLABLE RECTIFIER CIRCUIT PHASE SHIFT CONTROL

Suppose the phase difference between the drive signals G_1 and G_4 of the power MOSFETs is θ, the phase difference between G_1 and G_2 is π and the phase difference between G_3 and G_4 is π, then the phase difference between G_1 and G_3 should be (π-θ). In addition, the drive signal G_1 is in phase with the current $\boldsymbol{I}_a$ on the AC side of the rectifier circuit. The waveform of the driving signal is shown in Figure 4.

$$\theta = \pi - 2\alpha \tag{21}$$

Therefore, there is a relationship between the conduction angle and the phase shift angle in (21). From (19), the relationship between the phase shift angle and the equivalent impedance Z_{eq} can be obtained as (22). The relationship of charging voltage and charging current as a function of phase shift angle are (23) and (24).

$$Z_{eq} = \frac{2(1+\cos\theta)^2 \sqrt{(\pi-\theta)(2-\cos\theta) - 3\sin\theta}}{\pi^{3/2}(\pi - \theta - \sin\theta)} R_L \tag{22}$$

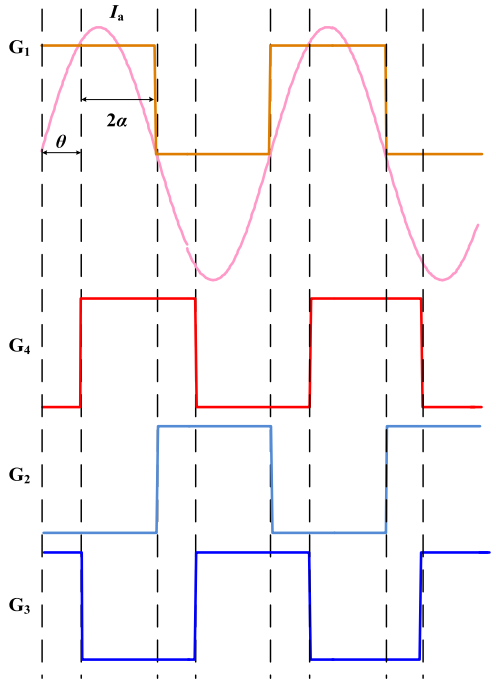

FIGURE 4. The waveforms of the driving signals.

$$I_L = \frac{\sqrt{2}MU_{im}(1+\cos\theta)}{\pi\omega L_1 L_2} \tag{23}$$

$$U_L = \frac{\sqrt{2}MU_{im}(1+\cos\theta)}{\pi\omega L_1 L_2} R_L \tag{24}$$

According to (23), the relationship between the phase shift angle and the charging current is:

$$\theta = \arccos\left(\frac{\pi\omega L_1 L_2 I_L}{\sqrt{2}MU_{im}} - 1\right) \tag{25}$$

The phase shift angle θ ranges from 0 to π. However, the value of θ should not be 0 to ensure the safety of the system and the value of θ is π at the time of system startup. From (25), we can see that the charging current is negatively related to θ.

According to the characteristics of constant current output of WPT system studied in this paper, it has little influence on the output current when the load changes within a certain range. In order to achieve the effect of rapid response, this paper adopts open-loop control for the CC charging. The current controller can calculate the phase-shifting angle of the rectifier circuit according to the charging current I_d of the load demand. Then, four PWM signals are generated from the value of the phase shift angle and delivered to the drive circuit of the four Power MOSFETs, thereby realizing the control of constant current charging.

The voltage closed-loop control is adopted for the CV charging. The demand voltage U_d is used as the reference voltage U_d^* for the closed-loop control. The charging voltage U_L is collected and compared with the reference voltage U_d^* in real time. The PI regulator is used for adjustment, and

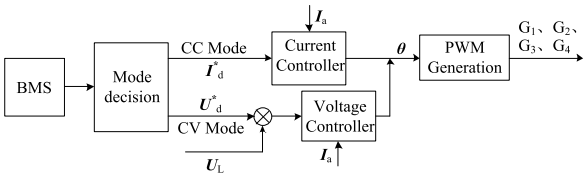

FIGURE 5. The control block of the CC and CV mode.

then four PWM signals are generated which is sent to the drive circuit of the Power MOSFETs, thus realizing constant voltage charging.

The whole control block diagram is shown in Figure5. It should be noted that in the actual application of the electric vehicle wireless charging system, the charging mode is determined by the battery management system (BMS). The BMS determines which charging mode to adopt based on the battery SOC, battery voltage and other information. Then the electric vehicle sends the command to wireless charging system (CC charging with I_d or CV charging with U_d). In addition, it is necessary to use a sensor to detect the phase of the current $\boldsymbol{I}_a$, so that the phase of the driving signal G_1 is in phase with it.

B. THE EFFICIENCY OPTIMIZATION STRATEGY BASED ON DYNAMIC EQUIVALENT IMPEDANCE MATCHING

It should be noted that the premise of the efficiency optimization strategy mentioned in this paper is that there is a certain range of load demand. That is, the actual charging current or charging voltage of CC mode or CV mode can fluctuate within a certain range. As long as it is in the required area, it can be called constant voltage or constant current charging, which is also reasonable in practical applications.

During the constant current charging process, the required current value is known as I_d^*, and the tolerable charging fluctuation rate is $\delta_1\%$. Namely, the range of charging current is $(1-\delta_1\%)I_d$ to $(1+\delta_1\%)I_d$. The control flow chart of efficiency optimization is shown in the Figure 6, and the specific optimization process is as follows:

Step 1: Initialize the system and determine the system parameters of $U_i, f_o, L_1, L_2, I_d, \delta_1, R_t, R_r$.

Step 2: Detect the current $\boldsymbol{I}_a$ of the inductor L_2, and obtain the mutual inductance value M from (9). Then calculate the optimal equivalent impedance value Z_{eq_m} from (15). Detect the charging voltage U_L and charging current I_L, and obtain the current phase shift angle θ_t and the phase shift angle range are θ_{min} to θ_{max} according to (25).

Step 3: The current equivalent impedance value $Z_{eq}(t)$ and equivalent impedance range are Z_{eq_min} to Z_{eq_max} can be obtained from (22).

Step 4: If $Z_{eq}(t)$ is less than Z_{eq_m} and Z_{eq_max} is less than Z_{eq_m}, the WPT system performs constant current charging at the phase shift angle θ_{min}. If $Z_{eq}(t)$ is less than Z_{eq_m} but Z_{eq_max} is greater than Z_{eq_m}, then the controller reduces the phase shift angle by a certain step size $\Delta\theta$ until the equivalent

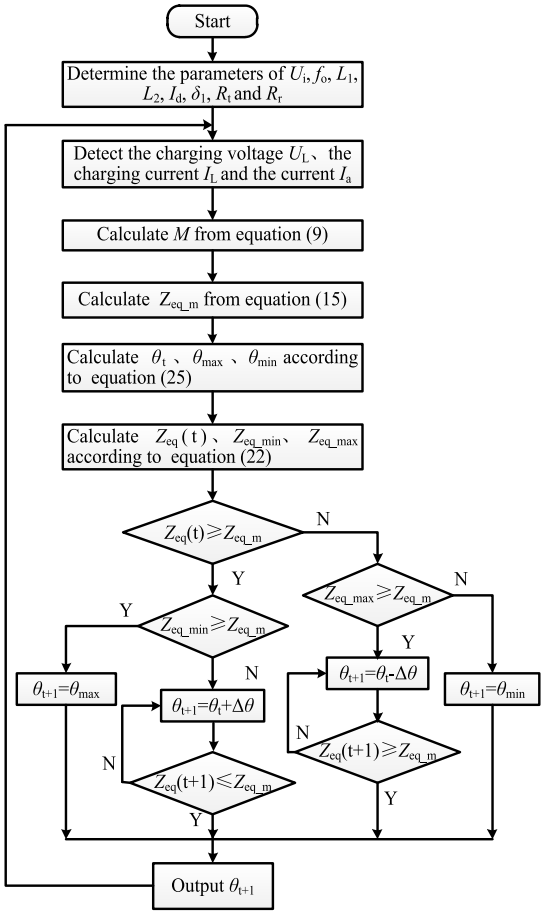

FIGURE 6. Flow chart for efficiency optimization of CC charging.

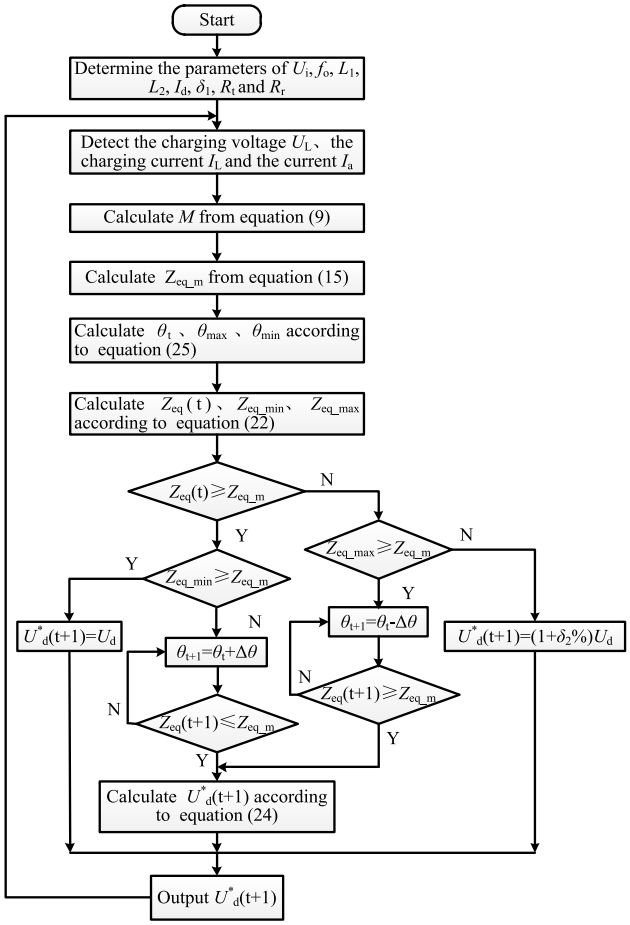

FIGURE 7. The flow chart for efficiency optimization of CV charging.

impedance $Z_{eq}(t+1)$ at the next moment is equal to the optimal equivalent impedance. Finally, output the phase shift angle θ_{t+1} and the system charges the load with maximum transmission efficiency.

Step 5: If $Z_{eq}(t)$ is greater than Z_{eq_m} and Z_{eq_min} is greater than Z_{eq_m}, the WPT system performs constant current charging at the phase shift angle θ_{max}. If $Z_{eq}(t)$ is greater than Z_{eq_m} but Z_{eq_min} is less than Z_{eq_m}, then the controller system increases the phase shift angle by a certain step $\Delta\theta$ until the equivalent impedance $Z_{eq}(t+1)$ at the next moment is equal to the optimal equivalent impedance and the system charges the load with maximum transmission efficiency.

For the efficiency optimization of the CV charging process, the control idea is similar to CC charging, but the actual charging voltage will not be lower than the demand voltage. Suppose the tolerable charging voltage fluctuation rate is $\delta_2\%$, then the range of charging voltage is U_d to $(1+\delta_2\%)U_d$. Since the CV mode adopts closed-loop control, the reference voltage U_d^* changes dynamically during the optimization process. The control flow chart for efficiency optimization of CV mode is shown in Figure 7, and the specific optimization process is as follows:

Steps 1, **Step 2** and **Step 3** are consistent with the CC model, which will not be repeated here.

Step 4: If $Z_{eq}(t)$ is less than Z_{eq_m} and Z_{eq_max} is less than Z_{eq_m}, the WPT system performs $(1+\delta_2\%)U_d$ as the reference voltage for CV charging. If $Z_{eq}(t)$ is less than Z_{eq_m} but Z_{eq_max} is greater than Z_{eq_m}, then the controller reduces the phase shift angle by a certain step size $\Delta\theta$ until the equivalent impedance $Z_{eq}(t+1)$ at the next moment is equal to the optimal equivalent impedance. The value of reference voltage U_d^* (t+1) is obtained from (12). Finally, output the reference voltage U_d^* (t+1) and the system charges and the system charges the load with maximum transmission efficiency.

Step 5: If Z_{eq} is greater than Z_{eq_m} and Z_{eq_min} is greater than Z_{eq_m}, the WPT system performs U_d as the reference voltage for CV charging. If Z_{eq} is greater than Z_{eq_m} but Z_{eq_min} is less than Z_{eq_m}, then the controller system increases the phase shift angle by a certain step $\Delta\theta$ until the equivalent impedance $Z_{eq}(t+1)$ at the next moment is equal to the optimal equivalent impedance. The value of reference voltage U_d^* (t+1) is obtained from (24). Finally, output the reference voltage U_d^* (t+1) and the system charges the load with maximum transmission efficiency.

TABLE 1. Parameters of the simulation and experiment for the WPT system.

Parameters	Simulation values	Experiment values
U_{DC}	167 V	167 V
f_o	85 kHz	86.5 kHz
M/h	M=20 μH	h=15 cm
L_t	103.5 μH	103.5 μH
L_r	92.9 μH	92.9 μH
R_t	0.168 Ω	0.168 Ω
R_t	0.178 Ω	0.178 Ω
L_1	20 μH	24.21 μH
C_1	175.3 nF	175.32 nF
C_t	41.99 nF	42.02 nF
L_2	28 μH	31.67 μH
C_2	125.21 nF	124.5 nF
C_r	54.02 nF	54.72 nF
R_L	CC mode 5 Ω~20 Ω CV mode 20 Ω~60 Ω	CC mode 5 Ω~20 Ω CV mode 20 Ω~30 Ω

This paper takes the LCC compensation topology as an example to analyze and propose the charging control strategy, but it is also applicable to other compensation topologies. For the WPT systems with different compensation topologies, the corresponding charging control strategy can be studied with reference to the control strategy proposed in this paper.

IV. SIMULATION AND EXPERIMENTAL VALIDATION

The simulation and experiment are carried out in this paper in order to verify the effectiveness of the proposed control strategy. The parameters of the WPT system are shown in Table 1. The parameters of simulation and those of experiment in this paper are basically the same. The input of the system is the DC voltage source, which becomes the high-frequency AC square wave after passing through the high-frequency inverter. In addition, to be equivalent to U_{im} as the input, the DC voltage needs to meet (26).Set the input voltage $U_{im} = 150$V, then the value of DC voltage $U_{DC} = 167$V.

$$U_{DC} = \frac{\pi}{2\sqrt{2}} U_{im} \approx 1.11 U_{im} \tag{26}$$

A. SIMULATION ANALYSIS

In this paper, the simulation software of MATLAB/Simulink was used for verification and analysis. The value of mutual induction M was set as 20 μH. Figure 8 shows the waveform of the current $\boldsymbol{I}_a$ and four-channel PWM signal. It can be seen that the phases of the current $\boldsymbol{I}_a$ and the PWM signals of G_1 are consistent, and the system operating frequency is 85 kHz.

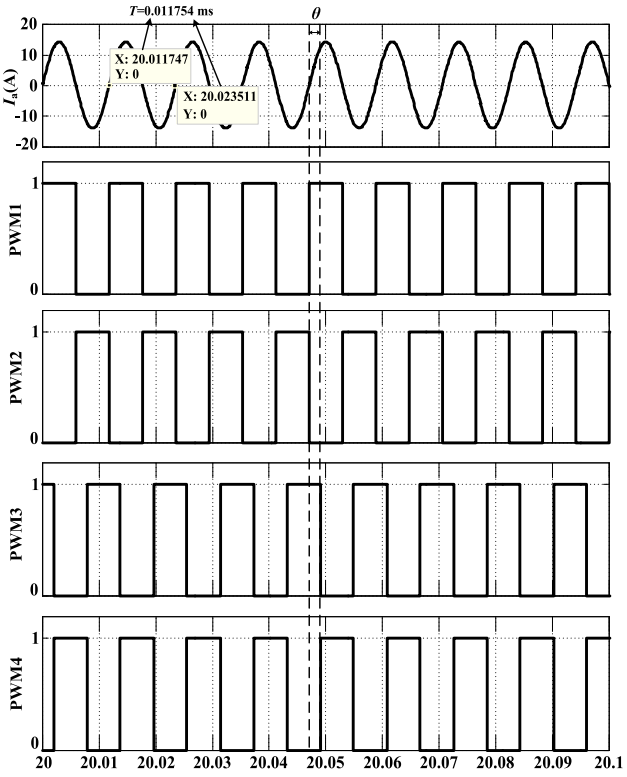

FIGURE 8. The simulation waveforms of current I_a and four-channel PWM signal.

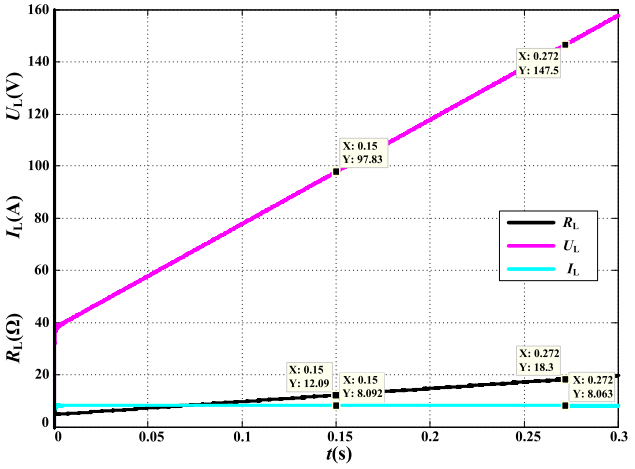

FIGURE 9. The simulation waveforms of the charging voltage and charging current during the increase of load resistance in CC mode.

The charging current of CC mode is set to 8A, and the charging voltage of CV mode is set to 160V. The tolerable fluctuation rate is 10%, then the charging current range of CC mode is 7.2 A to 8.8 A, and the charging voltage range of CV mode is 160 V to 176 V. This paper simulates continuous time-varying resistance as a simulated load in MATLAB/Simulink using a controlled current source, which can achieve the effect of rapid change of load resistance. Figure 9 shows the charging current and charging voltage in

CC mode during the process of increasing load resistance. It can be seen from the figure 9 that when the load resistance changes from 12.09 Ω to 18.3 Ω, the charging voltage increases from 97.83 V to 147.5 V and the charging current is basically unchanged, thus achieving the control of constant current charging. It also shows that the proposed control method has strong robustness.

The switching point for CC mode to CV mode in this paper is determined by the charging voltage value. When the charging voltage is greater than 160 V, the CC mode is switched to the CV mode, as shown in Figure 10. It can be seen from the figure 10 that during the change of the load resistance from 20.45 Ω to 40.21 Ω, the charging current gradually decreased from 7.824 A to 3.991 A, while the charging voltage is basically unchanged, indicating that the proposed control method has strong robustness in CV mode.

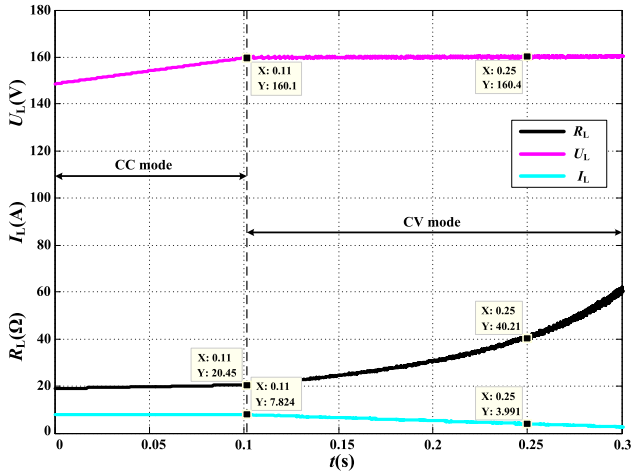

FIGURE 10. The simulation waveforms of the charging voltage and charging current waveforms during the increase of load resistance.

This paper also carried out simulation verification on the proposed efficiency optimization strategy. It should be noted that the transmission efficiency is generally calculated by measuring the power of the AC terminal of the high-frequency inverter and the power of the AC terminal of the secondary-side rectifier circuit. However, both ends are high-frequency alternating current, and the measured power is not very accurate, resulting in inaccurate data on transmission efficiency. Therefore, this paper measures the power of the DC input terminal and the load side to calculate the overall efficiency η_o of the system. In practical applications, people are more concerned about the overall efficiency of the WPT system, so this paper ultimately improves the overall efficiency of the system by optimizing the transmission efficiency.

In the CC mode and the value of load resistance is 5 Ω, the overall efficiency η_o is calculated by measuring the voltage and current values on the input and output sides. The overall efficiency η_o is 84.11% without the efficiency optimization strategy. When the efficiency optimization strategy

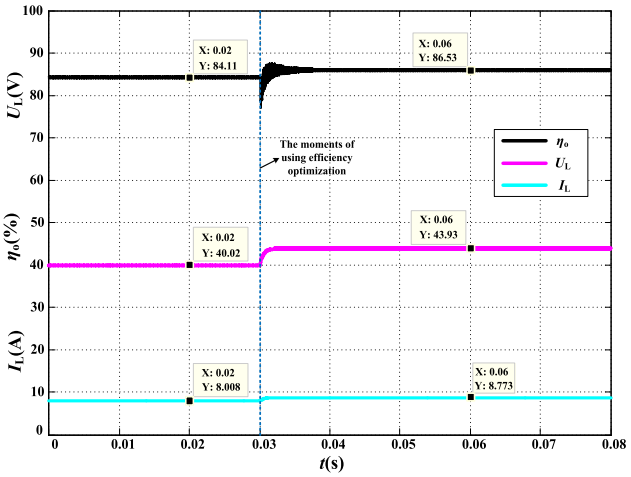

FIGURE 11. The simulation waveforms of charging current, charging voltage and overall efficiency before and after efficiency optimization in CC mode.

mentioned in this paper is used, the charging current changes from 8.008A to 8.773A, and the overall efficiency η_o increases to 86.53%, as shown in Figure 11.

In the CV mode and the load resistance value is 25 Ω, the current and voltage values of the input and output are measured separately to calculate the overall efficiency η_o. The overall efficiency η_o is 93.14% without the efficiency optimization strategy. When the efficiency optimization strategy mentioned in this paper is adopted, the charging voltage changes from 160.2 V to 175.1 V, and the overall efficiency η_o increases to 93.71%, as shown in Figure 12.

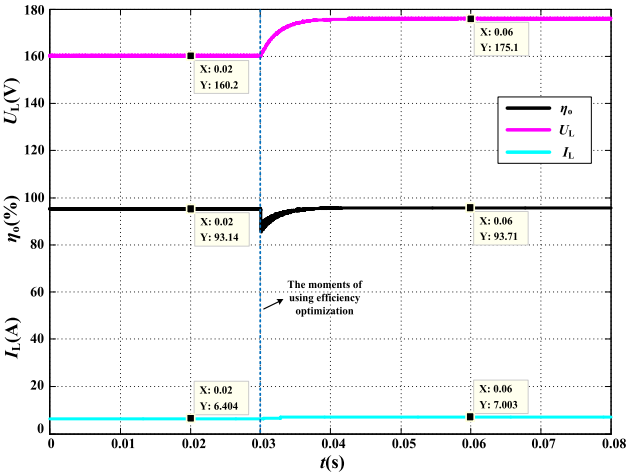

FIGURE 12. The simulation waveforms of charging current, charging voltage and overall efficiency before and after efficiency optimization in CV mode.

After simulating different load resistance values, the following conclusions are found under the WPT system structure and parameters studied in this paper:

1) In CC mode, the load resistance value is smaller, and the optimization effect is more obvious.

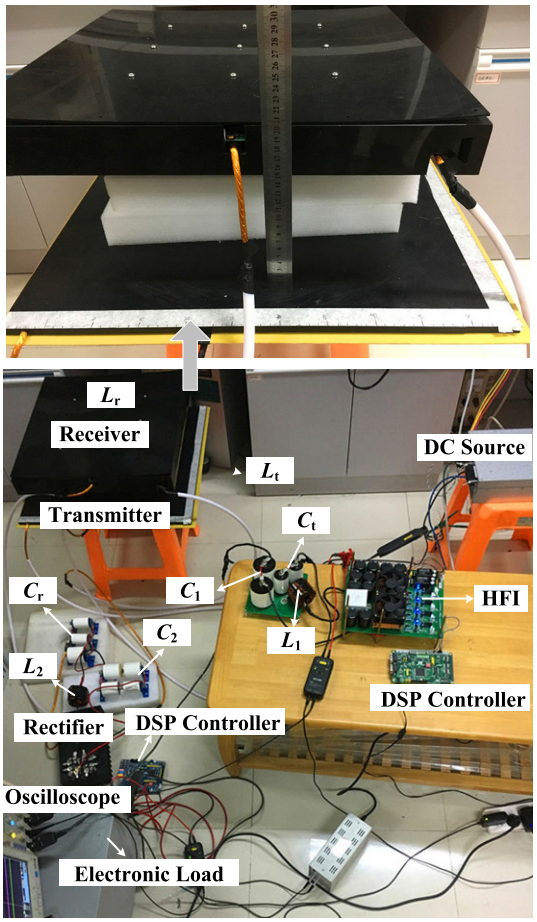

FIGURE 13. The WPT system experimental platform with a structure of double-sided LCC compensation topology and containing controllable rectifier circuit at the secondary side.

2) In CV mode, the load resistance value is larger than that in CC mode, and the efficiency η_o will be relatively high without optimization. There will be a slight increase after adopting the efficiency optimization strategy in this paper.

3) The system has better stability during dynamic load changes by using the proposed control strategy.

B. EXPERIMENTAL ANALYSIS

This paper also built the WPT system experimental platform with a structure of double-sided LCC compensation topology and containing full-bridge controllable rectifier circuit at the secondary side in order to verify the effectiveness of the proposed control strategy, as shown in Figure 13. The input is the DC voltage source (U_{DC} = 167V), which is converted into high-frequency alternating current through full-bridge inverter circuits (SiC Power MOSFETs: IXYS IXFN50N120SiC). Then through the magnetic coupling resonators with the transmission distance of 15 cm, full-bridge rectifiers (SiC Power MOSFETs: IXYS IXFN50N120SiC) and capacitor filter. Finally, it provides to the DC electronic load (Chroma 63212A-1200-480). The controllers of the primary-side full-bridge inverter and the secondary-side full-bridge rectifier are both use the DSP (TMS320F28335). The transmitter coil and the receiver coil are wound by the Litz wire (φ 0.1 mm × 1750 strands, outer φ 6.3 mm).

In the CC mode, the load resistance is adjusted from 5 Ω to 20 Ω during the experiment. It can be seen from Figure 14 that the charging voltage increases from 42.5 V to 165 V, and the charging current is basically unchanged which achieving the effect of constant current charging. In addition, the system responds quickly and fluctuates less during load changes. It also shows that the proposed control method still has strong robustness when the load impedance changes suddenly in CC mode.

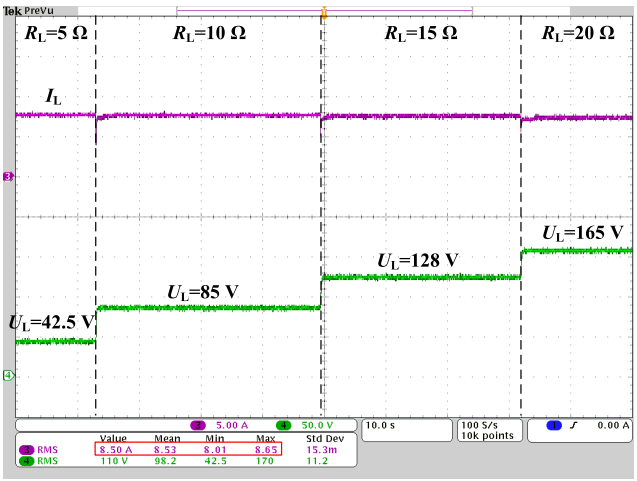

FIGURE 14. The experimental waveforms of I_L and U_L during the increase of load resistance in CC mode.

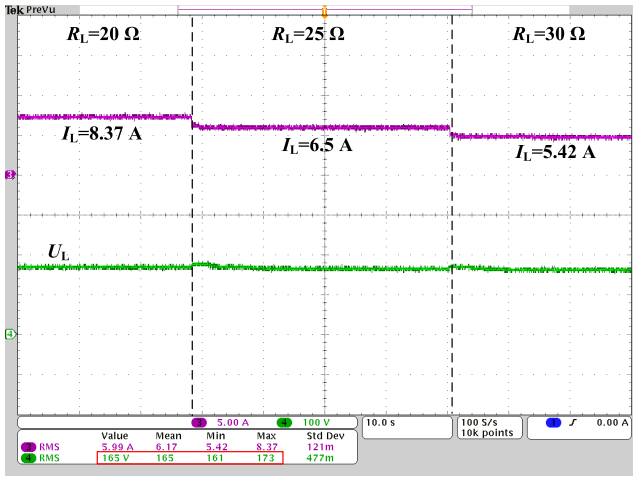

FIGURE 15. The experimental waveforms of I_L and U_L during the increase of load resistance in CV mode.

In CV mode, the experiment adjusts the load resistance from 20 Ω to 30 Ω. As can be seen from Figure 15, the charging current drops from 8.37 A to 5.42 A while the charging voltage is basically unchanged. In addition, the small voltage fluctuation when the load impedance changes suddenly in

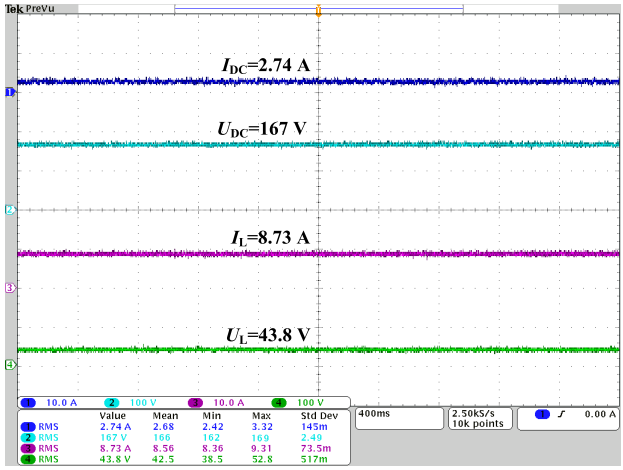

FIGURE 16. The experimental waveforms of I_{DC}, U_{DC}, I_L and U_L in CC mode.

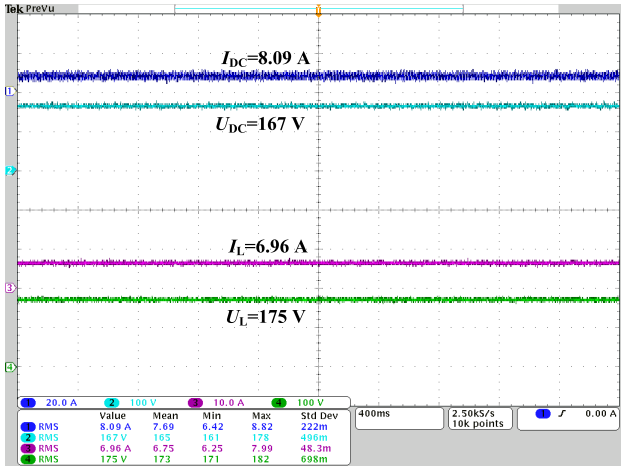

FIGURE 17. The experimental waveforms of I_{DC}, U_{DC}, I_L and U_L in CV mode.

CV mode indicate that the proposed control method has strong robustness.

The following experiments verify the effectiveness of the efficiency optimization strategy proposed in this paper. In the CC mode, the resistance of the electronic load is set to 5 Ω. Detecting the voltage and current of the input and output terminals after adopting the efficiency optimization strategy proposed in this paper, the input power $P_{DC} = 457.6$ W and the charging power $P_L = 382.4$ W, then the overall efficiency of the system is 83.57%, as shown in Figure 16. In the CV mode, the value of the load resistance is 25 Ω. The voltage and current of the input and output terminals are detected, and the input power $P_{DC} = 1351$ W and the charging power $P_L = 1218$ W can be obtained by calculation, then the system overall efficiency is 90.15%, as shown in Figure 17. It should be noted that the simulation data does not take into account the loss of high-frequency inverter, the rectifier and other components, so the experimental data is slightly lower than the simulation data. It should be noted that the power of the

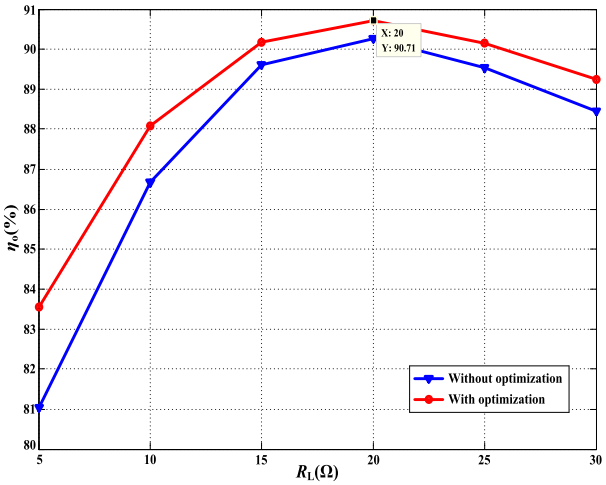

FIGURE 18. The comparison chart of the system overall efficiency with optimization and without optimization.

experiment in this paper is kW level, but it is also suitable for applications that require higher power (wireless charging of electric vehicles).

The following is the comparison chart of the system overall efficiency with optimization and without optimization, as shown in Figure 18. In the process of load resistance change, the overall efficiency after using the optimization strategy proposed in this paper can reach up to 90.71%. The optimization effect is more obvious in the area with smaller load resistance. The system can achieve higher efficiency if the magnetic coupling mechanism is optimized, which will be the focus of future research. The advantage of this method is that it can improve the overall efficiency of the WPT system while achieving CC and CV charging, without the need for communication between the primary side and the secondary side. The control method is simple and highly reliable.

V. CONCLUSION

In this paper, the control strategy to realize CC/CV charging and efficiency optimization is proposed for the WPT system with a structure of double-sided LCC compensation topology and containing controllable rectifier circuit at the secondary side. Based on this, the efficiency optimization strategies are proposed for CC mode and CV mode. Firstly, the expressions of the optimal transmission efficiency, the optimal equivalent impedance, and the equivalent impedance of the capacitor-filtered full-bridge controllable rectifier are derived through theoretical analysis. The relationship between the charging current and the phase shift angle of the secondary-side rectifier circuit is also obtained. Then, the CC/CV control strategy based on the phase-shift control of the controllable rectifier circuit and the efficiency optimization strategy based on dynamic equivalent impedance matching are proposed. Finally, the correctness and effectiveness of the proposed control strategy are verified by means of simulation and experiment. During the changes of the load from 5 Ω to 30 Ω,

the CC mode and the CV mode can be realized respectively. And when the parameter of load resistance changes, the WPT system can still maintain stability under the proposed control strategy. In addition, the WPT system overall efficiency after using the optimization strategy can reach up to 90.71% at the transmission distance of 15cm.

REFERENCES

[1] H. H. Lee, S. H. Kang, and C. W. Jung, "MR-WPT with reconfigurable resonator and ground for laptop application," *IEEE Microw. Wireless Compon. Lett.*, vol. 28, no. 3, pp. 269–271, Mar. 2018.

[2] K. Bao, C. L. Zekios, and S. V. Georgakopoulos, "A wearable WPT system on flexible substrates," *IEEE Antennas Wireless Propag. Lett.*, vol. 18, no. 5, pp. 931–935, May 2019.

[3] H. Liu, X. Huang, L. Tan, J. Guo, W. Wang, C. Yan, and C. Xu, "Dynamic wireless charging for inspection robots based on decentralized energy pickup structure," *IEEE Trans. Ind. Informat.*, vol. 14, no. 4, pp. 1786–1797, Apr. 2018.

[4] R. Mai, Y. Chen, Y. Li, Y. Zhang, G. Cao, and Z. He, "Inductive power transfer for massive electric bicycles charging based on hybrid topology switching with a single inverter," *IEEE Trans. Power Electron.*, vol. 32, no. 8, pp. 5897–5906, Aug. 2017.

[5] C. Liu, C. Jiang, J. Song, and K. T. Chau, "An effective sandwiched wireless power transfer system for charging implantable cardiac pacemaker," *IEEE Trans. Ind. Electron.*, vol. 66, no. 5, pp. 4108–4117, May 2019.

[6] L. Tan, M. Zhang, S. Wang, S. Pan, Z. Zhang, J. Li, and X. Huang, "The design and optimization of a wireless power transfer system allowing random access for multiple loads," *Energies*, vol. 12, no. 6, p. 1017, Mar. 2019.

[7] H. Zeng, S. Yang, and F. Z. Peng, "Design consideration and comparison of wireless power transfer via harmonic current for PHEV and EV wireless charging," *IEEE Trans. Power Electron.*, vol. 32, no. 8, pp. 5943–5952, Aug. 2017.

[8] Y. Bu, S. Endo, and T. Mizuno, "Improvement in the transmission efficiency of EV wireless power transfer system using a magnetoplated aluminum pipe," *IEEE Trans. Magn.*, vol. 54, no. 11, pp. 1–5, Nov. 2018.

[9] Y. Yao, Y. Wang, X. Liu, K. Lu, and D. Xu, "Analysis and design of an S/SP compensated IPT system to minimize output voltage fluctuation versus coupling coefficient and load variation," *IEEE Trans. Veh. Technol.*, vol. 67, no. 10, pp. 9262–9272, Oct. 2018.

[10] S. Ruddell, U. K. Madawala, and D. J. Thrimawithana, "Dynamic WPT system for EV charging with integrated energy storage," *IET Power Electron.*, vol. 12, no. 10, pp. 2660–2668, Aug. 2019.

[11] M. Kim, D.-M. Joo, and B. K. Lee, "Design and control of inductive power transfer system for electric vehicles considering wide variation of output voltage and coupling coefficient," *IEEE Trans. Power Electron.*, vol. 34, no. 2, pp. 1197–1208, Feb. 2019.

[12] K. Song, Z. Li, J. Jiang, and C. Zhu, "Constant current/voltage charging operation for series–series and series–parallel compensated wireless power transfer systems employing primary-side controller," *IEEE Trans. Power Electron.*, vol. 33, no. 9, pp. 8065–8080, Sep. 2018.

[13] A. Berger, M. Agostinelli, S. Vesti, J. A. Oliver, J. A. Cobos, and M. Huemer, "A wireless charging system applying phase-shift and amplitude control to maximize efficiency and extractable power," *IEEE Trans. Power Electron.*, vol. 30, no. 11, pp. 6338–6348, Nov. 2015.

[14] F. Liu, Y. Yang, Z. Ding, X. Chen, and R. M. Kennel, "A multifrequency superposition methodology to achieve high efficiency and targeted power distribution for a multiload MCR WPT system," *IEEE Trans. Power Electron.*, vol. 33, no. 10, pp. 9005–9016, Oct. 2018.

[15] Y. Chen, H. Zhang, S.-J. Park, and D.-H. Kim, "A switching hybrid LCC-S compensation topology for constant current/voltage EV wireless charging," *IEEE Access*, vol. 7, pp. 133924–133935, 2019.

[16] Y. Yao, Y. Wang, X. Liu, F. Lin, and D. Xu, "A novel parameter tuning method for a double-sided LCL compensated WPT system with better comprehensive performance," *IEEE Trans. Power Electron.*, vol. 33, no. 10, pp. 8525–8536, Oct. 2018.

[17] M. Fu, C. Ma, and X. Zhu, "A cascaded boost–buck converter for high-efficiency wireless power transfer systems," *IEEE Trans. Ind. Informat.*, vol. 10, no. 3, pp. 1972–1980, Aug. 2014.

[18] Y. Li, J. Hu, F. Chen, Z. Li, Z. He, and R. Mai, "Dual-phase-shift control scheme with current-stress and efficiency optimization for wireless power transfer systems," *IEEE Trans. Circuits Syst. I, Reg. Papers*, vol. 65, no. 9, pp. 3110–3121, Sep. 2018.

[19] V.-B. Vu, D.-H. Tran, and W. Choi, "Implementation of the constant current and constant voltage charge of inductive power transfer systems with the double-sided LCC compensation topology for electric vehicle battery charge applications," *IEEE Trans. Power Electron.*, vol. 33, no. 9, pp. 7398–7410, Sep. 2018.

[20] Y. Li, J. Hu, X. Li, F. Chen, Q. Xu, R. Mai, and Z. He, "Analysis, design, and experimental verification of a mixed high-order compensations-based WPT system with constant current outputs for driving multi-string LEDs," *IEEE Trans. Ind. Electron.*, vol. 67, no. 1, pp. 203–213, Jan. 2020.

[21] Y. Wang, Y. Yao, X. Liu, D. Xu, and L. Cai, "An LC/S compensation topology and coil design technique for wireless power transfer," *IEEE Trans. Power Electron.*, vol. 33, no. 3, pp. 2007–2025, Mar. 2018.

[22] W. Zhang and C. C. Mi, "Compensation topologies of high-power wireless power transfer systems," *IEEE Trans. Veh. Technol.*, vol. 65, no. 6, pp. 4768–4778, Jun. 2016.

[23] L. Yang, X. Li, S. Liu, Z. Xu, C. Cai, and P. Guo, "Analysis and design of three-coil structure WPT system with constant output current and voltage for battery charging applications," *IEEE Access*, vol. 7, pp. 87334–87344, 2019.

[24] X. Wang, J. Xu, M. Mao, and H. Ma, "An LCL-based SS compensated WPT converter with wide ZVS range and integrated coil structure," *IEEE Trans. Ind. Electron.*, early access, Apr. 28, 2020, doi: 10.1109/TIE.2020.2989707.

[25] Q. Zhao, A. Wang, J. Liu, and X. Wang, "The load estimation and power tracking integrated control strategy for dual-sides controlled LCC compensated wireless charging system," *IEEE Access*, vol. 7, pp. 75749–75761, 2019.

[26] J. Lu, G. Zhu, D. Lin, S.-C. Wong, and J. Jiang, "Load-independent voltage and current transfer characteristics of high-order resonant network in IPT system," *IEEE J. Emerg. Sel. Topics Power Electron.*, vol. 7, no. 1, pp. 422–436, Mar. 2019.

[27] H. Zhu, B. Zhang, and L. Wu, "Output power stabilization for wireless power transfer system employing primary-side-only control," *IEEE Access*, vol. 8, pp. 63735–63747, 2020.

[28] C. Cheng, F. Lu, Z. Zhou, W. Li, Z. Deng, F. Li, and C. Mi, "A load-independent LCC-compensated wireless power transfer system for multiple loads with a compact coupler design," *IEEE Trans. Ind. Electron.*, vol. 67, no. 6, pp. 4507–4515, Jun. 2020.

[29] W. Li, H. Zhao, J. Deng, S. Li, and C. C. Mi, "Comparison study on SS and double-sided LCC compensation topologies for EV/PHEV wireless chargers," *IEEE Trans. Veh. Technol.*, vol. 65, no. 6, pp. 4429–4439, Jun. 2016.

[30] G. V. Aparna, G. S. Babu, and T. M. Krishna, "Simulation and analysis of single phase full bridge diode rectifier with different passive power factor correction techniques," in *Proc. Int. Conf. Recent Innov. Electr., Electron. Commun. Eng. (ICRIEECE)*, Jul. 2018, pp. 2351–2355.

MING ZHANG (Graduate Student Member, IEEE) received the B.S. degree in electrical engineering and automation from Jiangsu Normal University, Xuzhou, China, in 2012, and the M.S. degree in electrical engineering from the Shanghai University of Electric Power, Shanghai, China, in 2015. He is currently pursuing the Ph.D. degree in electrical engineering with Southeast University, Nanjing, China.

His research interests include wireless power transfer and wireless charging for electric vehicles.

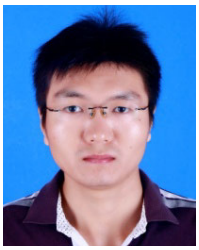

LINLIN TAN received the B.S. degree in electrical engineering and automation from Harbin Engineering University, Harbin, China, in 2008, and the Ph.D. degree in electrical engineering from Southeast University, Nanjing, China, in 2014.

He is currently an Associate Professor with the School of Electrical Engineering, Southeast University. He has published more than 20 articles. His current research interests include wireless power transfer, wireless charging for electric vehicles, and wireless V2G.

JIACHENG LI (Student Member, IEEE) received the B.S. degree in electrical engineering from Southwest Jiaotong University, Chengdu, China, in 2015. He is currently pursuing the Ph.D. degree in electrical engineering with Southeast University, Nanjing, China.

His research interests include wireless power transfer and numerical methods of electromagnetic field computation.

XUELIANG HUANG (Member, IEEE) received the B.S., M.S., and Ph.D. degrees in electrical engineering from Southeast University, Nanjing, China, in 1991, 1994, and 1997, respectively.

From 2002 to 2004, he held a postdoctoral position with The University of Tokyo. He has been a Professor with the Electrical Engineering Department, Southeast University, since 2004. He is the author of four books, more than 150 articles, and more than 40 inventions. He holds one PCT patent. His research interests include novel wireless power transfer systems, analysis of electromagnetic field, applied electromagnetics, intelligent electricity technology, and so on. He received the Teaching Achievement Prize of Jiangsu Province, in 2009, the Ministry of Environmental Protection Science and Technology Prize, in 2012, and so on. He serves as an Editor for Journal *Transactions of China Electrotechnical Society*.